***J. Ocean Univ. China*** (Oceanic and Coastal Sea Research)
https://doi.org/10.1007/s11802-021-4493-x
ISSN 1672-5182, 2021 20 (4): 790-802
*http://www.ouc.edu.cn/xbywb/*
*E-mail:xbywb@ouc.edu.cn*

# Adjoint Method-Based Algorithm for Calculating the Relative Dispersion Ratio in a Hydrodynamic System

JI Fei[1)], JIANG Wensheng[2), *], and GUO Xinyu[1), 3)]

1) *State Key Laboratory of Satellite Ocean Environment Dynamics*, *Second Institute of Oceanography*, *Ministry of Natural Resources*, *Hangzhou* 310012, *China*
2) *Key Laboratory of Marine Environment and Ecology (Ministry of Education of China)*, *Ocean University of China*, *Qingdao* 266100, *China*
3) *Center for Marine Environmental Studies*, *Ehime University*, *Matsuyama* 790-8577, *Japan*

(Received February 19, 2020; revised December 8, 2020; accepted April 9, 2021)


**Abstract** Relative dispersion ratio (RDR) can be used to quantify the deviation behavior of a water parcel's trajectory caused by a disturbance in a hydrodynamic system. It can be calculated by using a standard method for determining relative dispersion (RD), which accounts for the growth of the deviation of a cluster of particles from a specific initial time. However, the standard method for computing RD is time consuming. It involves numerous computations on tracing many water parcels. In this study, a new method based on the adjoint method is proposed to acquire a series of RDR fields in one round of tracing. Through this method, the continuous variation in the RDR corresponding to a time series of the disturbance time $t$ can be obtained. The consistency and efficiency of the new method are compared with those of the standard method by applying it to a double-gyre flow and an unsteady Arnold-Beltrami-Childress flow field. Results show that the two methods have good consistency in a finite time span. The new method has a notable speedup for evaluating the RDR at multiple $t$.

**Key words** relative dispersion; particle tracking; adjoint method; computational efficiency

## 1 Introduction

Particle tracking is widely used in oceanographic studies involving either *in situ* observation or numerical simulation. Its applications include rescue, marine oil spill detection, and marine environmental research (Hackett *et al.*, 2009; García-Garrido *et al.*, 2015; Kim *et al.*, 2015). A good example of applying water parcel tracking is the autonomous Lagrangian current explorer float, which also plays an important role in ocean observations, such as the global ARGO program (Davis *et al.*, 1992). Particle tracking is also used to find the source of certain substances distributed in seawater through backward tracking in various areas, including coasts and oceans (Durgadoo *et al.*, 2017; Gelderloos *et al.*, 2017).

However, with particle tracking, a small disturbance on particles (either temporal or spatial) may cause a large path deviation. Particles released almost simultaneously at nearly the same location will exhibit dispersion behavior (Batchelor, 1952; Kuznetsov *et al.*, 2002; LaCasce, 2008). Particles are normally assumed to be moving with the flow; as such, dispersion reflects the character of the flow field. Thus, the trajectory of a single particle is insufficient to represent the complete information about mass transport in seas. As a result, particle dispersion, which is caused by some mechanisms such as mixing in a hydrodynamic system, is also defined to characterize material transport and advection velocity (LaCasce and Ohlmann, 2003; LaCasce, 2008).

To quantify the dispersion effect during particle tracking, Batchelor (1952) proposed the concept of relative dispersion (RD). LaCasce (2008) provided a simpler form that is described by releasing a cluster of particles in the vicinity of $\boldsymbol{x}_0$ at the initial time $t_0$. The RD of point $t_0$ at time $T$ with disturbance at $t_0$ is defined in Eq. (1) as the variance of the displacement of that cluster of particles

$$D(T, \boldsymbol{x}_0, t_0) = \frac{1}{N(N-1)} \sum_{\substack{i \neq j \\ 1 \le i, j \le N}} \left\| \boldsymbol{x}(T, \boldsymbol{x}_{i0}, t_0) - \boldsymbol{x}(T, \boldsymbol{x}_{j0}, t_0) \right\|^2, \quad (1)$$

where $N$ is the total number of particles in a release experiment, $t_0$ is the releasing time, $\boldsymbol{x}_{i0}$ ($1 \le i \le N$) is the releasing position of the $i$th particle at the initial releasing time $t_0$ in the vicinity of $\boldsymbol{x}_0$. The operator $\| \|$ is the norm in an $n$-dimensional Euclidean space and denotes the separation of particles from the center of mass (Batchelor, 1952). $\boldsymbol{x}(T, \boldsymbol{x}_{i0}, t_0)$ is the position of the particle at time $T$

* Corresponding author. Tel: 0086-532-66782977
E-mail: wsjang@ouc.edu.cn

released at $\boldsymbol{x}_{i0}$ at the initial time $t_0$. If $\boldsymbol{x}_{i0}$ and $t_0$ are kept constant and only $T$ varies, $\boldsymbol{x}(T, \boldsymbol{x}_{i0}, t_0)$ represents the trajectory of the particle being released at position $\boldsymbol{x}_{i0}$ at time $t_0$. $T$, $\boldsymbol{x}_{i0}$ and $t_0$ are commonly separated with either '|' or ';' to reflect the Lagrangian characteristics and emphasize the varying feature of the variable $T$ and the fixing feature of the particle position $\boldsymbol{x}_{i0}$ at time $t_0$ in defining the trajectory. $T$. In this study $T$, $\boldsymbol{x}_{i0}$ and $t_0$ vary together, so neither '|' nor ';' is used to avoid confusion.

RD is an important index used to describe the characteristics of particle separation. First, the value of RD represents the repelling (or attracting) feature of particles in a flow field. Second, the change in RD over the time elapsed after a disturbance may reflect different dispersion mechanisms (Kraichnan, 1966; Bennett, 1984). For example, if dispersion is dominated by eddies with the same scale as the particle's separation distance, the growth of RD is in accordance with the power law. If dispersion is dominated by large-scale circulation, RD increases exponentially in time. If the separation between particles is larger than that in a circulation system, the motion of each particle shows an independent behavior that linearly increases RD with time. If the dispersion is caused by a random walk, RD is constant. Lastly, RD shows the sensitivity of a particle's trajectory to its initial state, *i.e.*, it is an index of the first kind of predictability (Lacorata *et al.*, 2014).

$\boldsymbol{D}(T, \boldsymbol{x}_0, t_0)$ depends on the initial distances among particles in a cluster. To eliminate the influence of the initial separation, we define the normalized RD as the relative dispersion ratio (RDR) as ,expressed as $\boldsymbol{D}(t, \boldsymbol{x}_0, t_0)/\boldsymbol{D}(t_0, \boldsymbol{x}_0, t_0)$, which is used to represent the dispersion feature of a flow field. The physical properties of RD (such as representing the repelling or attracting the features of particles and reflecting the mechanism of dispersion) can be inherited by the RDR. According to the form of the RDR, it is also an important intermediate variable, *i.e.*, the square of the amplification factor of the distance between the particle pairs in the calculation of the finite time Lyapunov exponent (FTLE; Pierrehumbert and Yang, 1993).

The RDR or the derived variable FTLE has been applied to many oceanography problems. Sanderson (2014) verified the interface between a river and an ocean in an estuary in terms of the RDR calculated from a 3D flow field. Cucco *et al.* (2016) used RDR to indicate the influence of wind data on the predictability of sea surface transport, which is crucial to maritime search and rescue operations. The spatial structure of the RDR is also utilized to explain water exchange in seas. For example, Fiorentino *et al*. (2012) applied this method and explained the mechanism of sewage accumulation in coast water. Using high-frequency radar data and high-resolution sea surface drifter data, Shadden *et al.* (2009) studied the exchange between water masses and calculated FTLE to verify the barrier effect of a high-FTLE ridge.

In observations and numerical experiments, the algorithm for calculating RD or RDR consists of two steps. First, a cluster of particles around one specific location is labeled at the initial time and each particle's exact position is retained. Second, the RD in Eq. (1) is calculated by recording the displacement of the particles in the cluster as time proceeds. This 'forward problem' framework can capture a series of subsequent effects of a single initial disturbance, but it needs a considerable computation effort. To find the RDR at one point, at least two particles are tracked through integration. Normally, RDR spatial coverage is required to analyze the dispersion behavior of a flow field, and a considerable number of particles are needed to be deployed in the study area. Consequently, this process requires numerous computation tasks. Furthermore, many time instances or time spans, namely $t_0$ and $T$, are required for the study, thereby enlarging the computation tasks.

In this study, a new method for calculating RDR is proposed by using the adjoint method to improve the computation efficiency of RDR. The adjoint method is a general approach to solve an inverse problem, which passes the derivative of one variable over state variables or some parameters backward to the whole process of a dynamic system (Le Dimet and Talagrand, 1986). In ocean studies, the adjoint method is widely utilized in sensitivity analysis, data assimilation, parameter estimation, optimal observation network design, and stability analysis (Errico, 1997; Daescu and Langland, 2013).

In this study, the RDR derived *via* the new method is called Adj-RDR to be distinguished from the RDR based on the traditional method. In one round of calculation, a series of Adj-RDR fields can be obtained on the basis of particle dispersions at the final time $T$ but with different initial time $t$. Thus, the potential disturbance at each time instance $t$ to the final position of the particle at time $T$ is determined. The new method is applied to two ideal flow fields to verify its consistency and efficiency.

The remaining parts of the paper are organized as follows. The existing RDR acquisition methods based on the definition and flow mapping are introduced in Section 2. The derivation of the new algorithm based on the adjoint method is also described in Section 2. Two ideal flow field experiments for the verification of our new method are demonstrated in Section 3. The results are discussed in Section 4, and the conclusions are presented in Section 5.

## 2 Methods

In Section 2.1, the standard RDR calculation method is presented to explain the new method. An algorithm based on flow mapping (Haller, 2002) is also proposed to extend the RDR as a continuous spatial function of the initial state. In Section 2.2, the new algorithm based on the adjoint method for calculating RDR is introduced.

### 2.1 RDR Calculation Based on a Standard Algorithm

The trajectory of a particle in a flow field is controlled by the following equation:

$$\frac{\partial \boldsymbol{x}}{\partial \tilde{t}} = \boldsymbol{u}(x(\tilde{t}, \tilde{\boldsymbol{x}}, t), t), \tag{2}$$

where $\boldsymbol{u}(\boldsymbol{x}(\tilde{t}, \tilde{\boldsymbol{x}}, t), \tilde{t})$ denotes the velocity of the particle

$(\tilde{\boldsymbol{x}},t)$ at time $\tilde{t}$. Its solution can be formally written as

$$\tilde{\boldsymbol{x}}_T = \boldsymbol{x}\left(T,\tilde{x},t\right) = \tilde{\boldsymbol{x}} + \int_t^T \boldsymbol{u}\left(\boldsymbol{x}\left(\tilde{t},\tilde{\boldsymbol{x}},t\right),\tilde{t}\right)\mathrm{d}\tilde{t}\,. \tag{3}$$

Eq. (3) can be regarded as the mapping of $\tilde{\boldsymbol{x}}$, the initial position of particle $(\tilde{\boldsymbol{x}},t)$ at time $t$ into its final position $\tilde{\boldsymbol{x}}_T$ at time $T$, which can be written as

$$\Phi_t^T : \tilde{\boldsymbol{x}} \to \tilde{\boldsymbol{x}}_T\,. \tag{4}$$

In Eq. (1), RD is calculated on the basis of the relative displacement among $N$ particles. It involves the distance between $N(N-1)/2$ pairs of particles. To simplify the derivation without losing generality, we define the distance of an arbitrary pair of particles as

$$\boldsymbol{d}_{i,j}\left(T,\boldsymbol{x}_0,t_0\right) = \left\|\boldsymbol{x}\left(T,x_{i0},t_0\right) - \boldsymbol{x}\left(T,x_{j0},t_0\right)\right\|^2,$$

so that $\boldsymbol{D}(T, \boldsymbol{x}_0, t_0)$ is the arithmetic mean of $\boldsymbol{d}_{i,j}(T, \boldsymbol{x}_0, t_0)$ and defined as

$$D\left(T,\boldsymbol{x}_0,t_0\right) = \frac{1}{N(N-1)} \sum_{\substack{i\neq j \\ 1\le i,j\le N}} d_{i,j}\left(T,\boldsymbol{x}_0,t_0\right).$$

According to this definition, the RDR is expressed in the form of

$$R\left(T,\boldsymbol{x}_0,t_0\right) = \frac{\sum_{\substack{i\neq j \\ 1\le i,j\le N}} d_{i,j}\left(T,\boldsymbol{x}_0,t_0\right)}{\sum_{\substack{i\neq j \\ 1\le i,j\le N}} d_{i,j}\left(t_0,\boldsymbol{x}_0,t_0\right)}.$$

If $\tilde{\boldsymbol{x}}$ is chosen near the point on the undisturbed trajectory $\boldsymbol{x}_t = \boldsymbol{x}(t, \boldsymbol{x}_0, t_0)$ when $\boldsymbol{x}_0$ and $t_0$ are fixed, then the two particles $(\tilde{\boldsymbol{x}},t)$ and $(\boldsymbol{x}_t, t)$ can form a particle pair, and their initial displacement is $\Delta\boldsymbol{x}_t = \tilde{\boldsymbol{x}} - \boldsymbol{x}_t$. At the final time $T$, their displacement is

$$\begin{aligned}\Delta\boldsymbol{x}\left(T,\boldsymbol{x}_t,t\right) &= \boldsymbol{x}\left(T,\tilde{\boldsymbol{x}},t\right) - \boldsymbol{x}\left(T,\boldsymbol{x}_t,t\right) \\ &= \boldsymbol{x}\left(T,\tilde{\boldsymbol{x}},t\right) - \boldsymbol{x}\left(T,\boldsymbol{x}_0,t_0\right),\end{aligned}$$

which can be expanded at $\boldsymbol{x}_t$ as

$$\Delta\boldsymbol{x}\left(T,\boldsymbol{x}_t,t\right) = \nabla\Phi_t^T\left(\boldsymbol{x}_t\right)\Delta\boldsymbol{x}_t + r\left(\Delta\boldsymbol{x}_t\right), \tag{5}$$

where $r(\Delta\boldsymbol{x}_t)$ is the residual term with $\lim_{\|\Delta\boldsymbol{x}_t\|\to 0} \frac{\|r(\Delta\boldsymbol{x}_t)\|}{\|\Delta\boldsymbol{x}_t\|} = 0$ and the Jacobian of the mapping is

$$\nabla\Phi_t^T\left(\boldsymbol{x}_t\right) = \begin{bmatrix} \dfrac{\partial x_1\left(T,\boldsymbol{x}_t,t\right)}{\partial x_1\left(t,\boldsymbol{x}_t,t\right)} & \cdots & \dfrac{\partial x_1\left(T,\boldsymbol{x}_t,t\right)}{\partial x_n\left(t,\boldsymbol{x}_t,t\right)} \\ \vdots & \ddots & \vdots \\ \dfrac{\partial x_n\left(T,\boldsymbol{x}_t,t\right)}{\partial x_1\left(t,\boldsymbol{x}_t,t\right)} & \cdots & \dfrac{\partial x_n\left(T,\boldsymbol{x}_t,t\right)}{\partial x_n\left(t,\boldsymbol{x}_t,t\right)} \end{bmatrix}, \tag{6}$$

where $\nabla\Phi_t^T(\boldsymbol{x}_t)$ describes the deformation rate of the infinitesimal perturbation of the initial position $\boldsymbol{x}_t$ or the development rate of the distance between two adjacent particles near $\boldsymbol{x}_t$.

Incorporating Eq. (5) into the matrix form of Eq. (1) obtains

$$d\left(T,\boldsymbol{x}_0,t_0\right) = \left[\Delta\boldsymbol{x}\left(T,\boldsymbol{x}_0,t_0\right)\right]^{\mathrm{T}} \cdot \Delta\boldsymbol{x}\left(T,\boldsymbol{x}_0,t_0\right), \tag{7}$$

where $[\ ]^{\mathrm{T}}$ denotes the transposition of a vector or a matrix.

When the higher-order infinitesimal is omitted, the RD of a particle pair with the initial distance $\Delta\boldsymbol{x}_t$ can be expressed as

$$d\left(T,\boldsymbol{x}_t,t\right) = \left[\Delta\boldsymbol{x}_t\right]^{\mathrm{T}}\left[\nabla\Phi_t^T\left(\boldsymbol{x}_t\right)\right]^{\mathrm{T}}\nabla\Phi_t^T\left(\boldsymbol{x}_t\right)\Delta\boldsymbol{x}_t\,. \tag{8}$$

$\boldsymbol{d}(T, \boldsymbol{x}_t, t)$ changes with the norm of disturbance $\|\Delta\boldsymbol{x}_t\|$ and the direction of disturbance $\Delta\boldsymbol{x}_t/\|\Delta\boldsymbol{x}_t\|$. Therefore, $\boldsymbol{R}(T, \boldsymbol{x}_0, t_0)$ is a statistical variable, although it is normalized with the arithmetic average of $d_{i,j}(t, \boldsymbol{x}_0, t_0) = \|\Delta\boldsymbol{x}_t\|^2$.

Haller (2002) provided a definition with a higher certainty by using the Cauchy-Green strain tensor at $\boldsymbol{x}_t$

$$C_{t_0}^T\left(\boldsymbol{x}_t\right) = \left[\nabla\Phi_t^T\left(\boldsymbol{x}_t\right)\right]^{\mathrm{T}}\nabla\Phi_t^T\left(\boldsymbol{x}_t\right). \tag{9}$$

The eigenvalue decomposition of $C_{t_0}^T(\boldsymbol{x}_t)$ can be expressed as

$$C_{t_0}^T\left(\boldsymbol{x}_t\right) = \begin{bmatrix}\xi_1 & \cdots & \xi_n\end{bmatrix}\begin{bmatrix}\lambda_1 & \cdots & 0 \\ \vdots & \ddots & \vdots \\ 0 & \cdots & \lambda_n\end{bmatrix}\begin{bmatrix}\xi_1 & \cdots & \xi_n\end{bmatrix}^{\mathrm{T}}, \tag{10}$$

where the eigenvalue $\lambda_i$ indicates the extension rate of the distance between the particles in a pair in the direction denoted by the eigenvector $\xi_i$.

Dispersion is led by the maximum eigenvalue in the direction of the corresponding eigenvector; as such, the maximum eigenvalue is often used as the index of the square of the amplification factor of the distance between the particles in a pair in the calculation of FTLE (Haller, 2002). In our study, the same notion is applied to calculate RDR:

$$\boldsymbol{R}(T,\boldsymbol{x}_t,t) = \max(\lambda_1,\lambda_2,\cdots,\lambda_n)\,. \tag{11}$$

The calculated $\boldsymbol{R}(T, \boldsymbol{x}_t, t)$ corresponds to the maximum RDR among all the initial displacement directions. In this study, the method described in this section is called the standard method.

### 2.2 RDR Calculation Based on the Adjoint Method

The above deduction reveals that if $\nabla\Phi_t^T(\boldsymbol{x}_t)$ is obtained, then the RDR along the trajectory can be acquired on the basis of dispersion from $t$ to $T$. However, in the standard RDR calculation described in Section 2.1, the independent integral of Eq. (3) is required to determine $\nabla\Phi_t^T(\boldsymbol{x}_t)$ for different values of $t$. This procedure needs numerous computation tasks to calculate the RDR for continuous $t$. Therefore, a new method based on the adjoint method is proposed to simplify the calculation.

First, a set of cost functions $J_k$, $k=1, 2,\cdots, n$ is defined as follows:

$$J_k(\boldsymbol{x},\tilde{\boldsymbol{x}}) = \mathrm{sign}\left(x_k(T,\tilde{\boldsymbol{x}},t) - x_k(T,\boldsymbol{x}_0,t_0)\right)\int_t^T \delta(\tilde{t}-T)\boldsymbol{\gamma}_k^{\mathrm{T}}\cdot\left(\boldsymbol{x}(\tilde{t},\tilde{\boldsymbol{x}},t) - \boldsymbol{x}(\tilde{t},\boldsymbol{x}_0,t_0)\right)\mathrm{d}\tilde{t}\ , \tag{12}$$

where $\boldsymbol{\gamma}_k = [\delta_{k1}, \delta_{k2},\cdots, \delta_{kn}]^{\mathrm{T}}$ with $\delta_{ki}$ being the Kronecker delta, $\delta(\tilde{t}-T)$ is the Dirac delta function, and sign( ) is the function that takes the sign of the variable with the absolute value of 1. It represents the distance between the two particles $(\boldsymbol{x}_0, t_0)$ and $(\tilde{\boldsymbol{x}},t)$ in the $k$th dimension at time $T$ which can be in its simple form:

$$J_k(\boldsymbol{x},\tilde{\boldsymbol{x}}) = \left|x_k(T,\tilde{\boldsymbol{x}},t) - x_k(T,\boldsymbol{x}_0,t_0)\right|. \tag{13}$$

Accordingly, a set of functionals with the constraints can be defined as

$$L_k(\boldsymbol{x},\boldsymbol{x}_k^*,\tilde{\boldsymbol{x}}) = J_k(\boldsymbol{x},\tilde{\boldsymbol{x}}) + \int_t^T [\boldsymbol{x}_k^*]^{\mathrm{T}}\cdot\left[\frac{\partial \boldsymbol{x}}{\partial\tilde{t}} - \boldsymbol{u}\left(\boldsymbol{x}(\tilde{t},\tilde{\boldsymbol{x}},t),\tilde{t}\right)\right]\mathrm{d}\tilde{t}\ , \tag{14}$$

where $\boldsymbol{x}_k^*(\tilde{t}) = [x_{k1}^*, x_{k2}^*,\cdots, x_{kn}^*]^{\mathrm{T}}$ is the vector of the Lagrangian multiplier and $k=1, 2,\cdots, n$.

$\boldsymbol{x}(\tilde{t},\tilde{\boldsymbol{x}},t)$ is the trajectory of particle $(\tilde{\boldsymbol{x}},t)$, as such, the second term of $L_k(\boldsymbol{x},\boldsymbol{x}_k^*,\tilde{\boldsymbol{x}})$ in Eq. (14) is always 0 because of Eq. (2). Therefore, we have

$$\nabla_{\tilde{\boldsymbol{x}}} L_k(\boldsymbol{x},\boldsymbol{x}_k^*,\tilde{\boldsymbol{x}}) = \nabla_{\tilde{\boldsymbol{x}}} J_k(\boldsymbol{x},\tilde{\boldsymbol{x}})\ . \tag{15}$$

If $\tilde{\boldsymbol{x}} \neq \boldsymbol{x}_t$, then

$$\nabla_{\tilde{\boldsymbol{x}}} J_k(\boldsymbol{x},\tilde{\boldsymbol{x}}) = \mathrm{sign}(x_k(T,\tilde{\boldsymbol{x}},t) - x_k(T,\boldsymbol{x}_0,t_0))\cdot \int_t^T \delta(\tilde{t}-T)\boldsymbol{\gamma}_k^{\mathrm{T}}\cdot\nabla_{\tilde{\boldsymbol{x}}}\boldsymbol{x}(\tilde{t},\tilde{\boldsymbol{x}},t)\mathrm{d}\tilde{t}\ . \tag{16}$$

Eq. (14) is integrated by parts to obtain

$$\begin{aligned} L_k\left(\boldsymbol{x},\boldsymbol{x}_k^*,\tilde{\boldsymbol{x}}\right) &= J_k + \left(\boldsymbol{x}^{\mathrm{T}}\cdot\boldsymbol{x}_k^*\right)\left(\boldsymbol{x}^{\mathrm{T}}\cdot\boldsymbol{x}_k^*\right)\Big|_t^T - \int_t^T\left[[\boldsymbol{x}]^{\mathrm{T}}\cdot\frac{\partial\boldsymbol{x}_k^*}{\partial\tilde{t}} + [\boldsymbol{x}_k^*]^{\mathrm{T}}\cdot\boldsymbol{u}\left(\boldsymbol{x}(\tilde{t},\tilde{\boldsymbol{x}},t),\tilde{t}\right)\right]\mathrm{d}\tilde{t} \\ &= J_k + \left[\boldsymbol{x}(T,\tilde{\boldsymbol{x}},t)\right]^{\mathrm{T}}\cdot\boldsymbol{x}_k^*(T) - [\tilde{\boldsymbol{x}}]^{\mathrm{T}}\cdot\boldsymbol{x}_k^*(t) - \int_t^T\left[\boldsymbol{x}^{\mathrm{T}}\cdot\frac{\partial\boldsymbol{x}_k^*}{\partial\tilde{t}} + \boldsymbol{x}_k^{*\mathrm{T}}\cdot\boldsymbol{u}\left(\boldsymbol{x}(\tilde{t},\tilde{\boldsymbol{x}},t),\tilde{t}\right)\right]\mathrm{d}\tilde{t}\ . \end{aligned} \tag{17}$$

When the Jacobi operator is applied to Eq. (17), and Eq. (16) is inserted, the following equation is derived:

$$\begin{aligned} \nabla_{\tilde{\boldsymbol{x}}} L_k\left(\boldsymbol{x},\boldsymbol{x}_k^*,\tilde{\boldsymbol{x}}\right) &= \left[\boldsymbol{x}_k^*(T)\right]^{\mathrm{T}}\cdot\nabla_{\tilde{\boldsymbol{x}}}\boldsymbol{x}(T,\tilde{\boldsymbol{x}},t) - \boldsymbol{x}_k^*(t) \\ &-\mathrm{sign}\left(x_k(T,\tilde{\boldsymbol{x}},t) - x_k(T,\boldsymbol{x}_0,t_0)\right)\int_t^T\left[\left[\frac{\partial\tilde{\boldsymbol{x}}_k^*}{\partial\tilde{t}}\right]^{\mathrm{T}} + \left[\tilde{\boldsymbol{x}}_k^*\right]^{\mathrm{T}}\cdot\nabla_{\boldsymbol{x}}\boldsymbol{u}\left(\boldsymbol{x}(\tilde{t},\tilde{\boldsymbol{x}},t),\tilde{t}\right) - \delta(\tilde{t}-T)\boldsymbol{\gamma}_k^{\mathrm{T}}\right]\cdot\nabla_{\tilde{\boldsymbol{x}}}\boldsymbol{x}(\tilde{t},\tilde{\boldsymbol{x}},t)\mathrm{d}\tilde{t}\ , \end{aligned} \tag{18}$$

where

$$\tilde{\boldsymbol{x}}_k^* = \mathrm{sign}\left(x_k(T,\tilde{\boldsymbol{x}},t) - x_k(T,\boldsymbol{x}_0,t_0)\right)\boldsymbol{x}_k^*\ .$$

If we set

$$\left[\frac{\partial\tilde{\boldsymbol{x}}_k^*}{\partial\tilde{t}}\right]^{\mathrm{T}} + [\tilde{\boldsymbol{x}}_k^*]^{\mathrm{T}}\cdot\nabla_{\boldsymbol{x}}\boldsymbol{u}\left(\boldsymbol{x}(\tilde{t},\tilde{\boldsymbol{x}},t),\tilde{t}\right) = \delta(\tilde{t}-T)\boldsymbol{\gamma}_k^{\mathrm{T}}\ , \tag{19}$$

with $\boldsymbol{x}_k^*(T) = 0$, *i.e.*, $\tilde{\boldsymbol{x}}_k^* = 0$, then Eq. (19) and its initial condition define a set of the adjoint functions of $\tilde{\boldsymbol{x}}_k^*$, so Eq. (18) becomes

$$\nabla_{\tilde{\boldsymbol{x}}} L_k\left(\boldsymbol{x},\boldsymbol{x}_k^*,\tilde{\boldsymbol{x}}\right) = -\boldsymbol{x}_k^*(t)\ .$$

Eq. (15) is transformed to

$$\nabla_{\tilde{\boldsymbol{x}}} J_k(\boldsymbol{x},\boldsymbol{x}_k^*,\tilde{\boldsymbol{x}}) = -\boldsymbol{x}_k^*(t)\ . \tag{20}$$

From Eq. (13), we can derive

$$\nabla_{\tilde{\boldsymbol{x}}} J_k = \mathrm{sign}\left(x_k(T,\tilde{\boldsymbol{x}},t) - x_k(T,\boldsymbol{x}_0,t_0)\right)\left[\frac{\partial x_k(T,\tilde{\boldsymbol{x}},t)}{\partial x_1(t,\tilde{\boldsymbol{x}},t)}\cdots\frac{\partial x_k(T,\tilde{\boldsymbol{x}},t)}{\partial x_n(t,\tilde{\boldsymbol{x}},t)}\right].$$

Comparing the above equation with Eq. (6), we can express the Jacobian matrix of the flow mapping $\nabla\Phi_t^T(\tilde{\boldsymbol{x}})$ as the gradient of the cost function, $\nabla_{\tilde{\boldsymbol{x}}} J_k$:

$$\nabla\Phi_t^T(\tilde{\boldsymbol{x}}) = \begin{bmatrix} \mathrm{sign}(x_1(T,\tilde{\boldsymbol{x}},t) - x_1(T,\boldsymbol{x}_0,t_0))\nabla_{\tilde{\boldsymbol{x}}} J_1{}^{\mathrm{T}} \\ \cdots \mathrm{sign}(x_n(T,\tilde{\boldsymbol{x}},t) - x_n(T,\boldsymbol{x}_0,t_0))\nabla_{\tilde{\boldsymbol{x}}} J_n{}^{\mathrm{T}} \end{bmatrix}^{\mathrm{T}}. \tag{11}$$

By inserting Eq. (20) into Eq. (21) and considering the definition of $\tilde{\boldsymbol{x}}_k^*$ we have

$$\nabla\Phi_t^T(\tilde{\boldsymbol{x}}) = -\left[\tilde{\boldsymbol{x}}_1^*(t),\cdots,\tilde{\boldsymbol{x}}_n^*(t)\right]. \tag{22}$$

In Eqs. (20) and (22), $\tilde{\boldsymbol{x}}$ cannot be $\boldsymbol{x}_t$, but we can evaluate $\nabla\Phi_t^T(\boldsymbol{x}_t)$ with $\nabla\Phi_t^T(\tilde{\boldsymbol{x}})$ when $\tilde{\boldsymbol{x}}$ is approaching $\boldsymbol{x}_t$. When Eqs. (19) and (22) are examined, no apparent restriction is imposed on $\tilde{\boldsymbol{x}} = \boldsymbol{x}_t$; thus, $\nabla\Phi_t^T(\boldsymbol{x}_t)$ can be expressed as

$$\nabla\Phi_t^T(\boldsymbol{x}_t) = -\left[\tilde{\boldsymbol{x}}_1^*(t),\cdots,\tilde{\boldsymbol{x}}_n^*(t)\right], \tag{23}$$

where $\tilde{\boldsymbol{x}}_k^*$ is obtained from Eq. (19) when $\tilde{\boldsymbol{x}}$ is set to $\boldsymbol{x}_t$ in that equation. Then, the RDR can be calculated with Eq. (11).

As an adjoint equation, Eq. (19) is numerically integrated from $\tilde{t}=T$ to $\tilde{t}=t_0$ with its initial condition $\tilde{\boldsymbol{x}}_k^*(T)=0$. The integration time range $[t_0, T]$ is split into $M$-1 sections with $\Delta t=(T-t_0)/(M-1)$.

Eq. (19) is separately integrated from $t_m=(m-1)\Delta t+t_0$ to $t_{m+1}=m\Delta t+t_0$ separately as follows:

$$\int_{t_m}^{t_{m+1}}\left[\left[\frac{\partial\tilde{\boldsymbol{x}}_k^*}{\partial\tilde{t}}\right]^{\mathrm{T}}+\left[\tilde{\boldsymbol{x}}_k^*\right]^{\mathrm{T}}\cdot\nabla_{\boldsymbol{x}}\boldsymbol{u}\left(\boldsymbol{x}\left(\tilde{t},\tilde{\boldsymbol{x}},t\right),\tilde{t}\right)\right]\mathrm{d}\tilde{t}=\int_{t_m}^{t_{m+1}}\delta\left(\tilde{t}-T\right)\boldsymbol{\gamma}_k^{\mathrm{T}}\mathrm{d}\tilde{t}\ .$$

The left-hand side is discretized with an implicit time-forward scheme. The right-hand side can be integrated analytically by considering a Dirac function in the integrand. Thus, the numerical scheme of Eq. (19) is expressed as follows:

$$\tilde{\boldsymbol{x}}_k^{*(m)}-\tilde{\boldsymbol{x}}_k^{*(m-1)}+\left[\nabla_{\tilde{\boldsymbol{x}}}\boldsymbol{u}^{(m)}\right]^{\mathrm{T}}\cdot\tilde{\boldsymbol{x}}_k^{*(m)}=\boldsymbol{\gamma}_k\delta_{mM},\quad m=1,2,\cdots,M\ ,\qquad(24)$$

where $\tilde{\boldsymbol{x}}_k^{*(m)}=\tilde{\boldsymbol{x}}_k^*((m-1)\Delta t+t_0)$ is the value of $\tilde{\boldsymbol{x}}_k^*$ defined at discrete temporal points, $t_m=(m-1)\Delta t+t_0$, $\boldsymbol{u}^{(\mathrm{m})}=\boldsymbol{u}(\boldsymbol{x}(t_m, \boldsymbol{x}_t, t), t_m)$, and $\delta_{mM}$ is the Kronecker delta. $\boldsymbol{x}_t$ is the position of the particle ($\boldsymbol{x}_0$, $t_0$) at time $t$, so $\boldsymbol{u}^{(m)}$ can also be expressed as $\boldsymbol{u}^{(m)}=\boldsymbol{u}(\boldsymbol{x}(t_m, \boldsymbol{x}_0, t_0), t_m)$.

If Eq. (24) is written in a matrix form under the initial condition of $\tilde{\boldsymbol{x}}_k^{*(M)}=0$, we have

$$\left[\tilde{\boldsymbol{x}}_1^{*(m-1)},\cdots,\tilde{\boldsymbol{x}}_n^{*(m-1)}\right]=\left(\boldsymbol{I}+\left[\nabla_{\boldsymbol{x}}\boldsymbol{u}^{(m)}\right]^{\mathrm{T}}\Delta t\right)\left[\tilde{\boldsymbol{x}}_1^{*(m)},\cdots,\tilde{\boldsymbol{x}}_n^{*(m)}\right]\quad m<M,\ (25)$$

and $\left[\tilde{\boldsymbol{x}}_1^{*(M-1)},\cdots,\tilde{\boldsymbol{x}}_n^{*(M-1)}\right]=-\boldsymbol{I}$.

Then, inserting Eq. (25) into Eq. (23), we can have the Jacobian of the mapping defined in Eq. (4) at different time steps $t_m$ along the trajectory, *i.e.*,

$$\nabla\Phi_{t_m}^T\left(\boldsymbol{x}_{t_m}\right)=\prod_{i=M-1}^{m}\left(\mathbf{I}+\left[\nabla_{\boldsymbol{x}}\boldsymbol{u}^{(i)}\right]^{\mathrm{T}}\Delta t\right).\qquad(26)$$

The RDR expressed in Eq. (11) can be obtained based on the Jacobian of flow mapping in Eq. (26). In this way, the influence of the disturbance at a series of time instance $t_m$ to the final location of the particle can be determined efficiently by evaluating the gradient of the flow field along the trajectory.

The calculation of RDR *via* the adjoint method can be divided into four steps:

1) Place a numerical particle on every grid point in the study area at a certain initial time.

2) Track each particle in the flow field from the initial time to the final time $T$, and keep the position of the particle at time $t_m$, $\boldsymbol{x}_{t_i}$ and $\nabla_{\boldsymbol{x}}\boldsymbol{u}^{(i)}$ at the same point at the same time, where $i=1, 2,\cdots, M$.

3) Calculate $\nabla\Phi_t^T(\boldsymbol{x}_t)$ according to Eq. (26) based on the information in step 2.

4) Calculate $C_{t_m}^T(\boldsymbol{x}_{t_m})$ according to Eq. (9) and obtain RDR based on Eq. (11).

However, $\boldsymbol{x}_{t_m}$ will not always be on the grid points similar to those at the beginning, and some particles may even leave the study area. The interpolation is also used to get RDR on each grid point.

## 3 Application of the Proposed Method in Two Ideal Flow Fields

In particle tracking studies, two common questions are commonly encountered. One is, 'what is the final particle distribution that can occur due to the disturbance at time (named as disturbance time $t_0$)?'. The other one is, 'what kind of disturbance at $t_0$ can cause the final distribution of particles?'. The first one is called the forward tracking problem, which can be used to describe the spreading of pollutants at a certain time (named as result time $T$) and being discharged at different $t_0$, *e.g.*, different phases of a tidal period. The second one is called the backward tracking problem, which can be utilized in instances such as locating the oil spill source at $t_0$ from the oil coverage in water at $T$. In both cases the final time $T$ is normally regarded as a fixed value, and $t_0$ is assumed as a varying variable. The RDR field at a continuously varying $t_0$ is required to solve these problems.

The RDR in the two problems can be obtained by using the traditional method described in Section 2.1. They can also be more efficiently solved by applying the new method presented in Section 2.2. In this section, two widely used analytical flow fields, namely, two-dimensional double-gyre flow and three-dimensional unsteady ABC flow, are adopted to verify the validity and efficiency of the new method proposed in Section 2.2. These flow fields are benchmark models for studying the Lagrangian chaos and mixing either 2D (Shadden *et al.*, 2005; Coulliette *et al.*, 2007) or 3D dynamic systems (Dombre *et al.*, 1986; Haller, 2001). In the present study, two-dimensional double-gyre flow and three-dimensional unsteady ABC flow are used in forward and backward tracking problems, respectively. The RDRs of these two flow fields at different initial times are calculated by using the standard method and the newly proposed adjoint method. The results of both methods are compared to verify the effectiveness of the new method.

For the convenience of reference, the RDRs calculated *via* the new method and the standard algorithm are called Adj-RDR and standard RDR, respectively.

### 3.1 Double-Gyre Flow Case

In this section, the forward tracking problem is solved for a double-gyre flow field. This flow field is designed as two adjacent closed gyres flowing at a constant speed. They are separated by a straight line named as the flow axis, which oscillates periodically with a small amplitude so that the two gyres can expand and contract alternately.

The flow field is given by

$$\begin{cases} u_1 = -\pi A \sin(\pi f(x_1,t))\cos(\pi x_2) \\ u_2 = \pi A \cos(\pi f(x_1,t))\sin(\pi x_2)\dfrac{\partial f(x_1,t)}{\partial x_1} \end{cases},$$

where

$$f(x_1,t) = a(t)x_1^2 + b(t)x_1,$$

$$a(t) = \varepsilon\sin(\omega t), \quad b(t) = 1 - 2\varepsilon\sin(\omega t).$$

In this study, the parameters are set as $\omega = 2\pi/10$, $\varepsilon = 0.1$, $A = 0.1$, *i.e.*, the period of the oscillation of the flow axis is 10 with an amplitude of 0.1 in the $\boldsymbol{x}_1$ direction, and the speed on the flow axis is 0.1, all variables in the ideal flow field are dimensionless. The calculation area is set as [0, 2] in the $\boldsymbol{x}_1$-axis direction and [0, 1] in the $\boldsymbol{x}_2$-axis direction. Resolution is set as $\Delta x_1 = \Delta x_2 = 0.002$ so that the grid number is 1000×500. The time step for obtaining the trajectory by integrating Eq. (3) is 0.002. In this study, a 4th-order predictor and a 5th-order corrector scheme are used to determine the integrals.

For calculating the RDR with the standard algorithm, particle pairs are released on the grid points with the initial displacement of $10^{-5}$. Six groups of experiments are set at $t_0 = 0$, 4, 8, 12, 16, 20 and $T = 20$. The results are displayed in column A of Fig.1, with the most remarkable feature of the double-gyre pattern. The high RDR occurs near the flow axis and forms several bands that stretch like a circle. The influence of the different values of $t$ can be found in column A in Fig.1 from rows 1 to 6. The high-value band between the two gyres moves left and right because of the oscillation of the flow axis. The integral time length also alters the pattern to some extent. The number of the high-RDR bands and the RDR in the band increase as the integral time is extended.

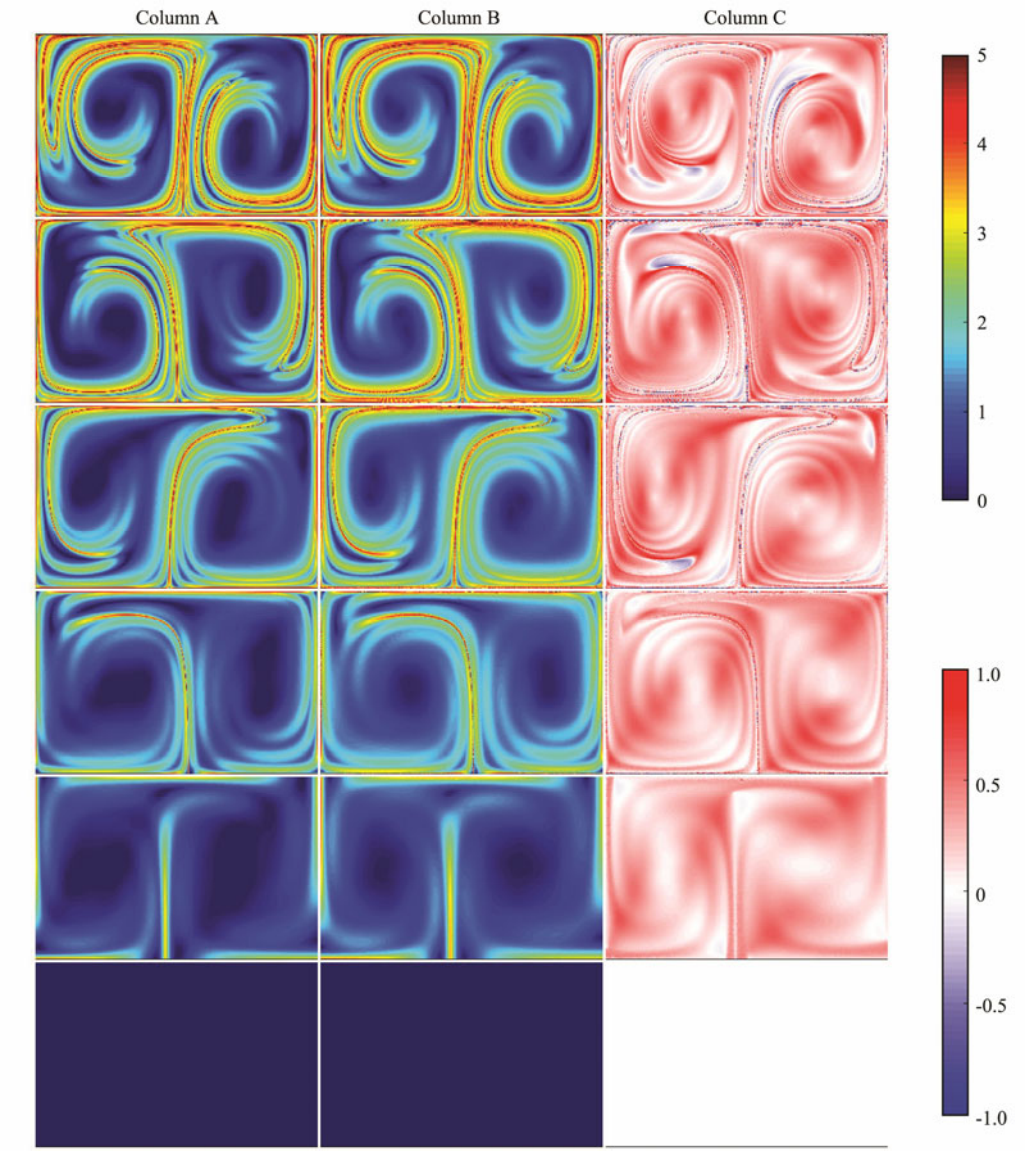


Fig.1 RDR of the double-gyre flow calculated by two methods. Column A, RDR calculated by the standard algorithm displayed as $\log_{10}$RDR; Column B, RDR calculated by the adjoint method, displayed as $\log_{10}$RDR; Column C, The absolute difference between RBR calculated by two methods. Rows 1 to 6 denote the results with initial disturbance time at 0, 4, 8, 12, 16 and 20.

Adj-RDR is calculated in accordance with the procedure described in Section 2.2 at a time step of 0.02. The reason for taking this value of $\Delta t$ is explained in the discussion. Six figures at $t_0=0$, 4, 8, 12, 16, 20 are selected and presented in column B of Fig.1, which shows the RDR distribution with the same meaning as those in column A. However, the RDRs of different $t_0$ are calculated by tracking the particles in one run. In Fig.1, the spatial pattern of Adj-RDR is consistent with the result of the standard algorithm. Their difference is less than 15% of the absolute value in column C of Fig.1, but Adj-RDR is higher than the result obtained *via* the standard algorithm. The overestimation of Adj-RDR occurs in the low-value region of RDR, *e.g.*, the center of the gyres. The difference between the two algorithms in a high-value area, where we are usually most interested in, is smaller than that in a low-value area. Therefore, the result of Adj-RDR is acceptable in the double-gyre test.

The area-averaged RDRs obtained with both methods are also compared in Fig.2. Adj-RDR is calculated at a time step interval of 0.02, so it is represented as a continuous line. The RDR based on the standard algorithm is shown as 6 points in the figure. When $t_0>8$, *i.e.*, the track span is shorter than 12, Fig.2 shows a good correspondence between the two RDRs based on different algorithms. The value produced *via* the new methodis higher than that obtained *via* the standard method. If $t_0<8$, *i.e.*, the track span is longer than 12, then Adj-RDR exponentially grows with the track span, but the standard RDR appears to reach the maximum value at $10^7$.

The computation time consumed by using the two methods is compared. A desktop computer with a 3.6 GHz AMD 3700x processor is used to calculate the RDR with MATLAB 2017b. 'Tic' and 'toc' commands are utilized to keep time. The computation time is the average of the results of three rounds of calculations. The standard method takes $138.1\pm0.5$ s to obtain the distribution of the RDR in six cases ($t_0=0$, 4, 8, 12, 16, 20). By comparison, the adjoint method needs $136.0\pm0.5$ s to determine the distribution of the RDR in 100 cases at $t_0$ of 0 to 20 with a time step of 0.2.

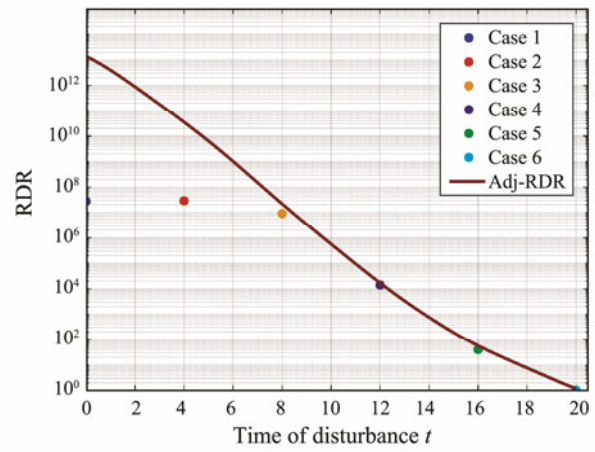


Fig.2 Area averaged RDRs calculated by both methods continuous line, Adj-RDR; point, RDR by standard algorism.

### 3.2 Backward Tracking in an Unsteady ABC Flow

As mentioned at the beginning of this section, the RDR can be used to determine the source of matter in oceans by solving the backward tracking problem. In the application of backward tracking, a new flow field is formulated by reversing the time sequence and taking the opposite sign of the original flow field. Thus, a new flow mapping is defined as

$$\Psi_T^t : \boldsymbol{x}_T \to \tilde{\boldsymbol{x}}. \tag{27}$$

Then, the RDR can be calculated for this flow mapping by using the standard algorithm or the adjoint method as the forward tracking problem.

The physical definition of the derived RDR differs from that obtained through forward tracking, as in Section 3.1. The high RDR, in this case, indicates the area where particles gather (Haller, 2015).

In this section, the unsteady ABC flow is used as the test flow field, which is given by

$$\begin{cases} u_1 = \left[A-\dfrac{1}{2}t\sin(\pi t)\right]\sin(x_3)-C\cos(x_2) \\ u_2 = \left[A-\dfrac{1}{2}t\sin(\pi t)\right]\cos(x_3)-B\cos(x_1) \\ u_3 = -C\cos(x_2)-B\cos(x_1) \end{cases}.$$

In this study, the parameters are set as follows: $A=-\sqrt{3}$, $B=-\sqrt{2}$, and $C=1$. The computational domain is in the cube $\{\boldsymbol{x}=(\boldsymbol{x}_1, \boldsymbol{x}_2, \boldsymbol{x}_3)|\ \boldsymbol{x}_i\in[0, 2\pi], i=1, 2, 3\}$ which is divided into 100×100×100 grids. The track span is set as 8, which is four periods of motion.

In the backward tracking problem, $t$ varies from $t_0=8$ to $T=0$. It can be transformed into a forward tracking problem by assuming that $\tilde{t}=t_0+T-t$, and the new velocity field is as follows:

$$\begin{cases} \tilde{u}_1 = -\left[A-\dfrac{1}{2}(8-\tilde{t})\sin(\pi(8-\tilde{t}))\right]\ \sin(x_3)+C\cos(x_2) \\ \tilde{u}_2 = -\left[A-\dfrac{1}{2}(8-\tilde{t})\sin(\pi(8-\tilde{t}))\right]\ \cos(x_3)+B\cos(x_1) \\ \tilde{u}_3 = C\cos(x_2)+B\cos(x_1) \end{cases}.$$

The original backward tracking problem here is to find the disturbance at $t$ that can generate the end state at $T$. In the transformed forward problem, the goal is to obtain the RDR when $\tilde{t}$ is from 0 to 8 and the final state is $\tilde{T}=8$. When the standard algorithm is used $\tilde{t}=0$, 0.4, 0.8, 1.2, 1.6, that corresponds to $\tilde{t}=8$, 7.6, 7.2, 6.8, 6.4 is chosen. When the new adjoint method is applied, $\tilde{t}$ is selected from 0 to 8 with a time step of 0.02.

The RDR distribution on the three surfaces of the calculation cube is shown in Fig.3 when $\tilde{t}=0$, *i.e.*, $t=8$ is chosen. The results from the standard algorithm and the

adjoint method are presented in Figs.3a and 3b, respectively. They display the 'hollow' pattern of a high value around the vortex tube. However, the RDR obtained with the adjoint method has a 'higher contrast' than that determined with the standard algorithm. Therefore, Adj-RDR is higher than the standard RDR in the high-value zone, whereas the former is lower than the latter in the low-value zone. This pattern can also be found in Fig.3c, which shows the difference between the RDRs acquired by both methods.

The RDR distribution at different initial times on the three slices in the middle of the cube, *i.e.*, $x_1=\pi$, $x_2=\pi$, and $x_3=\pi$, is plotted to express the results more clearly. The RDRs calculated by the standard algorithm and the adjoint method are displayed in Figs.4 and 5, respectively. Both RDR distributions are similar. However, the RDR in Fig.5 has a 'higher contrast' than that in Fig.4. Furthermore, the RDR distribution in Fig.5 becomes blurrier as the time span between $t_0$ and $T$ is prolonged.

The time series of area-averaged Adj-RDR and standard RDR are shown in Fig.6. Adj-RDR exponentially grows as $t$ increases. By comparison, the standard RDR grows exponentially when $t<6$; as it reaches the maximum value, it no longer grows as $t$ increases.

The time consumed by using the two methods in the ABC flow is compared. It is a 3D flow field, so the computation time is very long. For this reason, a parallel MATLAB m file is written and run in 10 threads. With the standard method, obtaining the RDR field in 1 case with $t=8$ takes 1331.3 s. With the adjoint method, determining the distribution of the RDR field in 400 cases with $t$ from 8 to 0 needs 2354.7 s.

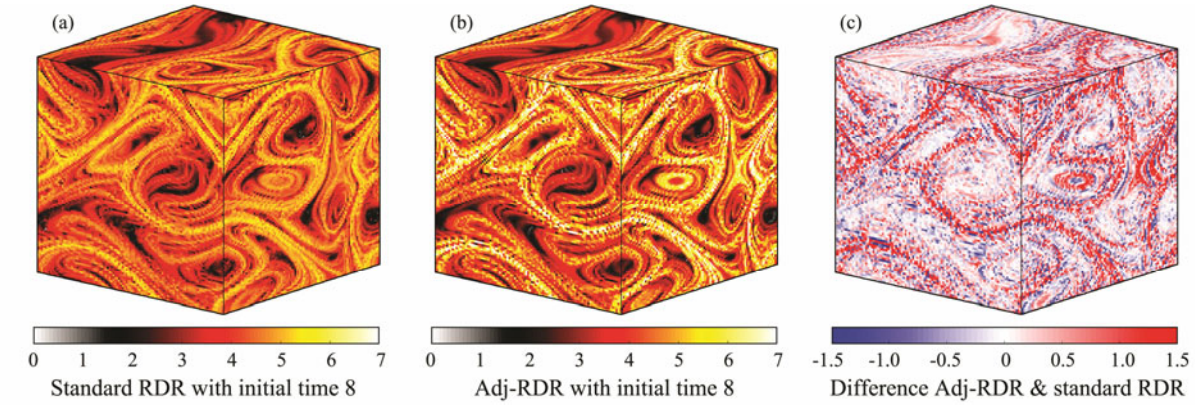


Fig.3 RDR distribution of unsteady ABC flow field on three surfaces of the cube. (a), RDR calculated by the standard algorithm as $\log_{10}$RDR; (b), RDR calculated by the adjoint method as $\log_{10}$RDR; (c), the absolute difference between RBR calculated by two methods time range is for $T=0$ and $t_0=8$.

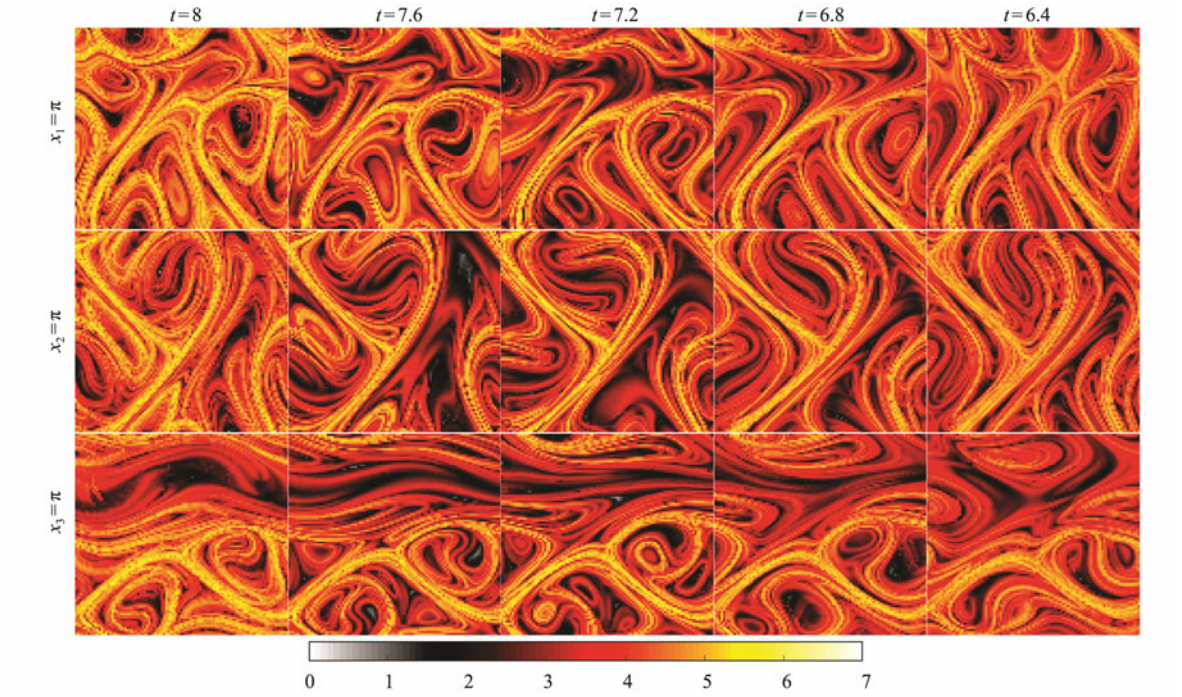


Fig.4 RDR distribution of unsteady ABC flow field calculated by the standard algorism on three inner sections of the cube with different initial time. The first row denotes $x_1=\pi$; second row denotes $x_2=\pi$; third row denotes $x_3=\pi$. The columns from 1–5 correspond to the initial time $t=8$, 7.6, 7.2, 6.8 and 6.4. The color in the figures denotes the value $\log_{10}$RDR.

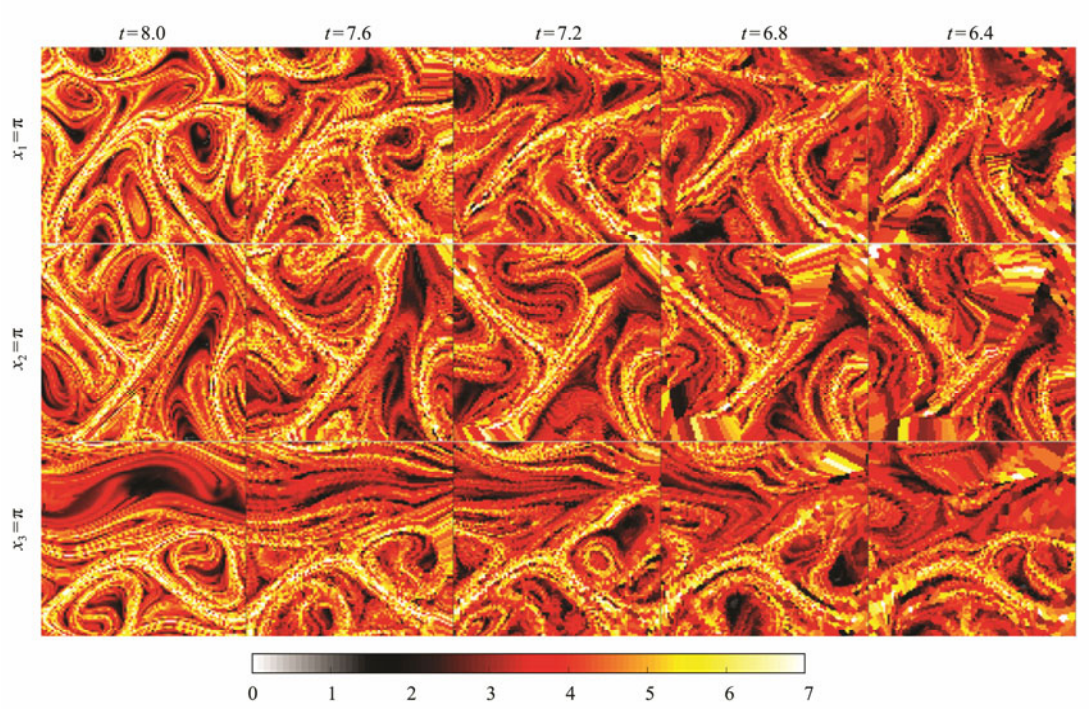


Fig.5 Same as Fig.4, but calculated by adjoint method.

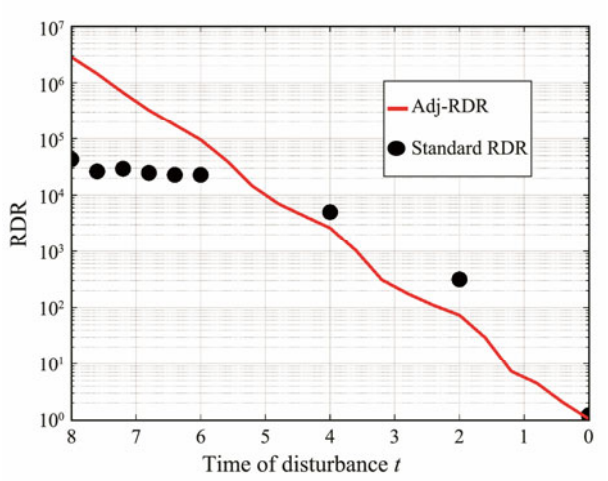


Fig.6 The time series of area-averaged Adj-RDR and standard RDR. The red line denotes the continuous time series of the sum of Adj-RDR change with different initial time and the black dots denotes the sum of RDR calculated by standard algorithm. Each dot is averaged from an independent experiment with the disturbed particles released at $t$.

## 4 Discussion

### 4.1 Computational Efficiency

The RDR field calculated with the adjoint method is almost continuous with respect to. By contrast, the RDR field obtained with the standard method is confined to a certain instance of $t$. The calculation procedure needs to be carried out several times to determine the influence of disturbance from time $t$ to $T$. Therefore, the new method is beneficial. The computational complexity of the two methods is briefly analyzed in this section.

In the standard method, particle tracking is the most time-consuming procedure. In the adjoint method, particle tracking and the calculation of Eq. (26) are both time consuming. Either particle tracking or particle tracking plus Eq. (26) consumes more than 90% of the calculation time of the corresponding method in the two examples in Section 3. Therefore, we focus on the comparison of the computational complexity of particle tracking and the calculation of Eq. (26).

The calculation cost of tracking one particle in an $n_d$-dimensional space in one time step needs at least $O(n_d^2)$ multiplications when a simple discrete form of Eq. (2), *i.e.*, Eq. (28), is used to track the particle:

$$\boldsymbol{x}^{(m+1)} = \left(\boldsymbol{I} + \nabla_{\boldsymbol{x}} \boldsymbol{u}^{(m+1)} \Delta t\right)^{\mathrm{T}} \boldsymbol{x}^{(m)}. \tag{28}$$

Every calculation of Eq. (28) is assumed as one unit of calculation here. By using the standard method, $n_d + 1$ particles should be tracked in the $n_d$-dimensional space to determine the RDR by calculating Eq. (6) at one point. If $n_t$ time steps are needed to track a particle from $t_0$ to $T$, then the computation cost to obtain $\boldsymbol{R}(T, \boldsymbol{x}_0, t_0)$ is $n_t \times (n_d + 1)$. The computation cost is $n_t \times (n_d + 1) \times n_r$ for the disturbance at a single time instance $t_0$ to determine the RDR field with $n_r$ sampling points. If a series of RDR fields is needed with respect to $n_c$ disturbance time instances, *e.g.*, the 6 cases in Section 3.1, $n_c$ independent calculations with different tracking time steps are needed. The disturbance time necessary. $t$ is spread evenly between $t_0$ to $T$ for $n_c$ cases. Then, the time step number in each case decreases from $n_t$ to 0, while $t$ is from $t_0$ to $T$. Therefore, the total computation time to complete the whole calculation is $n_c/2 \times n_t \times (n_d+1) \times n_r$.

In the adjoint method, the computation cost includes

the computation of Eq. (26) and the computation of particle tracking. The computation cost of Eq. (26) is $n_d$ times of Eq. (28). Particle tracking should be calculated from $t_0$ to $T$ ($n_t$ steps) and the calculation of Eq. (28) from $T$ to $t_0$ ($n_t$ steps) to acquire the RDR by using the adjoint method at one point. Therefore, for the continuous time series of Adj-RDR field at $n_r$ points, the computation cost is $n_t \times (n_d + 1) \times n_r$.

Theoretically, the adjoint method saves the computation cost $n_c/2$ times of that of the standard method in solving the inverse problem. In real calculation, the adjoint method needs to record and read the data of particle position and velocity, so the calculation time tends to be longer than the theoretical value. The speedup is less than $n_c/2$, but it is still very notable. In this study, the speedup ratio of the double-gyre example is about 16.9 times, which is less than 50 times in theory. For the unsteady ABC flow, the speedup ratio is about 113 times, which is also less than 200 times in theory.

In addition to time cost, the memory cost of the adjoint method is determined to calculate the RDR. The extra random-access memory (RAM) occupied by the Adj-RDR method mainly occurs in step 3 of the calculation procedure. In step 3, memory needs to save the spatial divergence tensor of the velocity for each particle of the current time step. The tensor is $d$ times larger than the velocity vector, where $d$ is the spatial dimension; as such, the RAM usage of step 3 is also $d$ times of the particle tracking process. For the double-gyre experiment in Section 3.1, the tensor takes up 15.305 megabytes of RAM.

Apart from the RAM usage, extra disk space is required in the Adj-RDR method to record the trajectory information compared with that in the standard method. The data size of the trajectory can be expressed as follows:

File's data size = Number of time steps × Number of released particles × Dimension of flow filed (float data).

The adjoint method requires a relatively high resolution in space and time, so the footprint of the trajectory information is a large amount of data. In the case of the double-gyre experiment in Section 3.1, the total size of the trajectory files is 6.872 gigabytes. In general, the extra cost of RAM and disk space is acceptable.

### 4.2 Computation Accuracy

Adj-RDR has the same spatial structure as that calculated by the standard algorithm in forward and backward tracking applications, as displayed in Section 3. However, Adj-RDR is higher than the standard RDR, especially when the calculation span is large. In the time series of the area-averaged Adj-RDR and standard RDR shown in Figs.2 and 6, Adj-RDR exponentially grows as the calculation time span increases. For the standard RDR, the dispersion ratio grows exponentially during a limited time; afterward, the area-averaged RDR appears to reach the maximum value. This difference occurs because the adjoint method calculates the tangent linear dispersion ratio in the smallest neighborhood along the particle trajectory. In the standard algorithm, the initial pair is finally separated into two tracks regardless of the size of the initial disturbance because of the effect of the dispersion. When the particle pairs are apart far enough, the relative motion between the particle pairs is basically random. Statistically, the average distance is no longer growing. Ding and Li (2007) explained the saturation phenomena in the study on the nonlinear FTLE. If the initial disturbance is small, the standard RDR is consistent with Adj-RDR in a longer time (Fig.7).

The RDR obtained by the adjoint method is sensitive to the time step in the calculation because of the tangent linear approximation. A set of experiments of the double-gyre flow field (as in Section 3.1) is used to discuss the relationship between the time step $\Delta t$ and the Adj-RDR. A standard algorithm with the initial disturbance $\delta \boldsymbol{x} = 10^{-5}$ is used as a benchmark result. Figs.8 and 9 illustrate the influence of different time steps on the difference in the two methods. The smaller the time step, the smaller the difference in the RDR between the two methods. Moreover, in Fig.9, the difference increases when $\Delta t = 0.032$. Thus, when $\Delta t$ is larger than the upper limit, the difference increases rapidly with $\Delta t$. However, when $\Delta t$ is less than the time step, the decrease in $\Delta t$ slightly affects the reduction in the difference. In the above experiment, $\Delta t = 0.02$ is used for the compromise between efficiency and accuracy.

Tangent linear approximation is introduced to Adj-RDR in the derivation of Eq. (24), and the second and higher-order term of $\Delta t$ is disregarded. Therefore, an upper limit of $\Delta t$ should be set to ensure that $\nabla_{\boldsymbol{x}} \boldsymbol{u}(\boldsymbol{x}(\tilde{t}, \boldsymbol{x}_t, t), \tilde{t})$ does not change significantly with $\Delta t$. The limit is also related to the characteristics of the flow field, *i.e.*, the temporal variation in $\nabla_{\boldsymbol{x}} \boldsymbol{u}(\boldsymbol{x}(\tilde{t}, \boldsymbol{x}_t, t), \tilde{t})$.

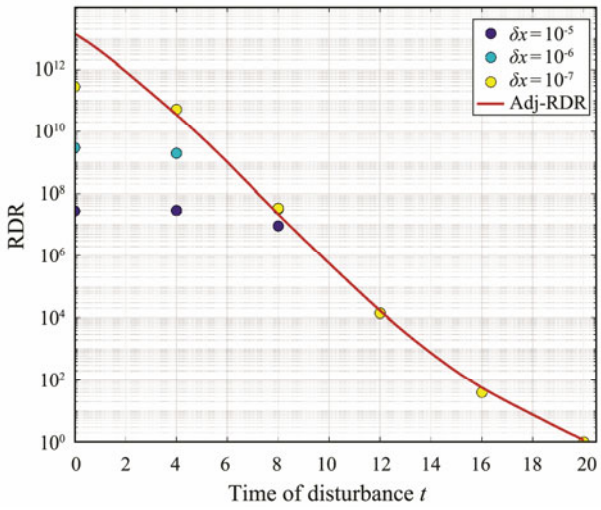


Fig.7 Same as Fig.2, but the results of the standard RDR with a smaller initial disturbance scale are supplemented. The red line represents the RDR at each initial time calculated by the adjoint algorithm. The blue, cyan, and yellow dots correspond to the RDR calculated by the standard algorithm, and the initial distances between the particle pairs are $10^{-5}$, $10^{-6}$, and $10^{-7}$, respectively.

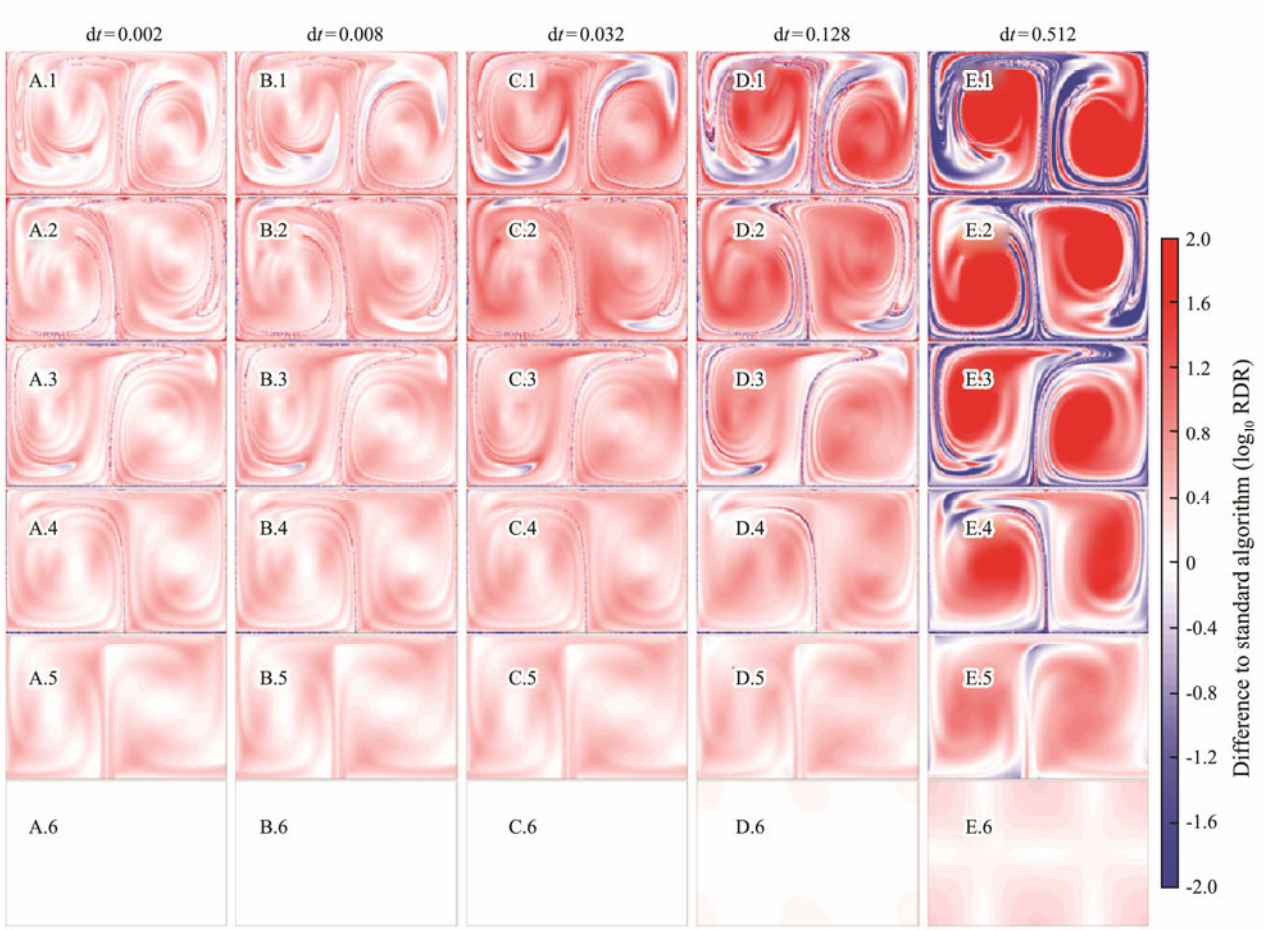


Fig.8 Absolute difference between Adj-RDR and standard RDR (Fig.1A). Columns A, B, C, D, and E denote the results obtained *via* the adjoint method with time steps of 0.002, 0.008, 0.032, 0.128, and 0.512, respectively. Rows 1 to 6 denote the results with initial disturbance times at 0, 4, 8, 12, 16, and 20.

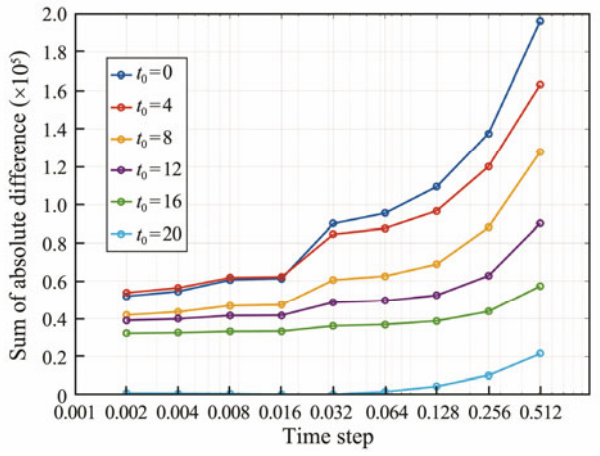


Fig.9 Sum of the absolute difference between Adj-RDR and standard RDR, and the change with time step.

### 4.3 Limitations of the New Method

The RDR calculated by the adjoint method is blurrier in distribution as the time span between $t_0$ and $T$ is prolonged (Fig.5). Therefore, the accuracy of the new method is limited when the time span is long.

The reason for the time span limitation is that $\boldsymbol{R}(T, \boldsymbol{x}_t, t)$ is calculated on the particle in the adjoint method, *i.e.*, RDR is mapped on $\boldsymbol{x}_t$, which varies with $t$. For comparison, in the standard method, RDR is mapped on the initial location where the particle is released. In an aperiodic flow field, when $t$ is farther away from $t_0$, $\boldsymbol{x}_t$ is farther away from the mesh point where the particles are released (Fig.10). In the area near the boundary, some particles leave the study area. In other words, the number of sampling points in the study area is reduced, and the distribution of sampling points is not uniform when $t-t_0$ is high. This effect is more significant for the flow field with an open boundary because particles eventually flow out of the study area.

However, if a study aims to calculate the structure of the RDR in a finite time, such as several tidal periods, the adjoint method is valid for the application.

## 5 Conclusions

In this study, a new method for calculating RDR is proposed by using the adjoint method. The validity of the method is verified *via* two idealized numerical experiments. The results reveal that the spatial structure of RDR calculated with the adjoint method is consistent with that obtained with the standard algorithm. The new method is successful in forward and backward tracking cases. Its

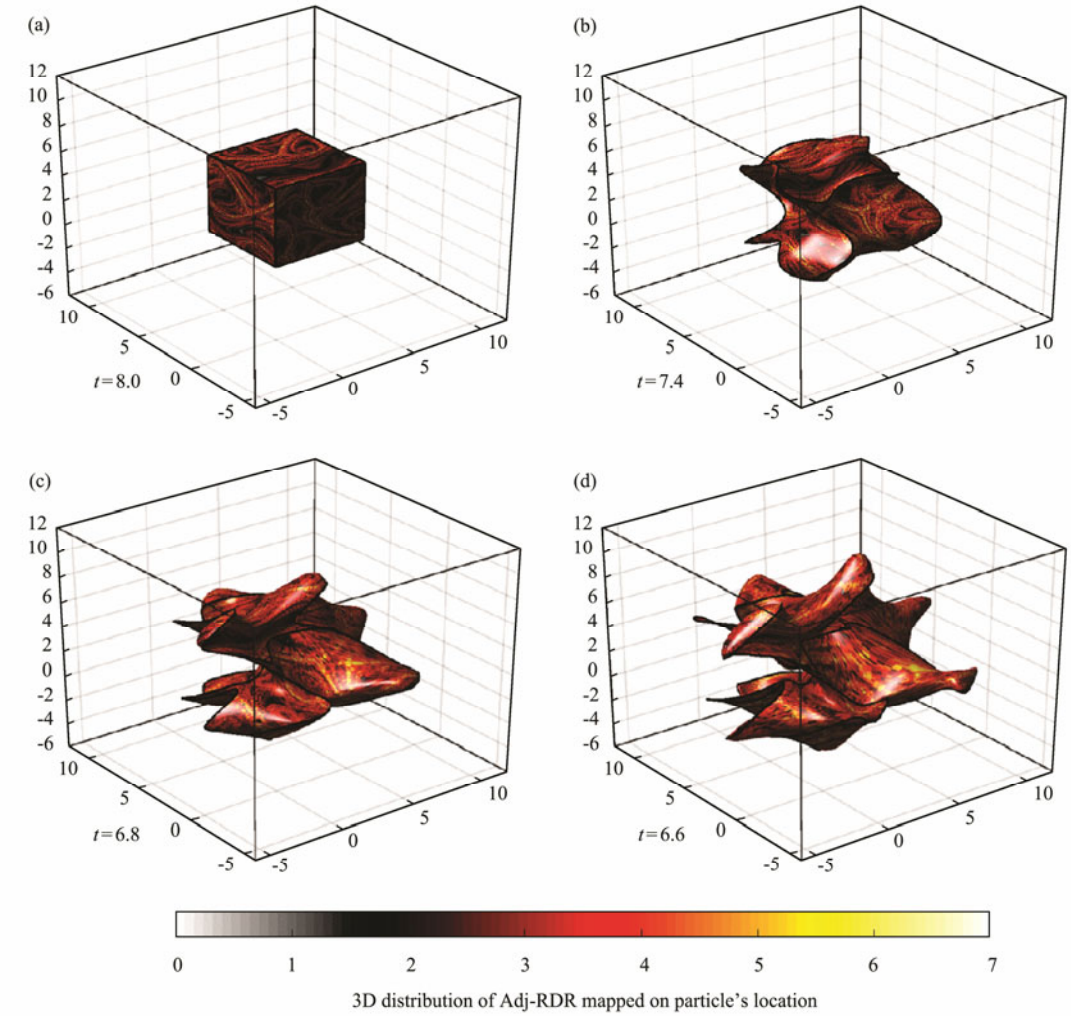


Fig.10 Adj-RDR distribution of the unsteady ABC flow field mapped on the location of a particle.

computational efficiency is also exhibited with a speedup of more than 15 times in the two examples.

The new method has some limitations. The spatial resolution of RDR decreases as the tracking time is extended. Moreover, RDR increases as the integration time is prolonged. In many cases, this limitation can be avoided because the RDR of a finite time is needed. RDR calculated for a long time loses its physical significance because of the nature of the flow field itself.

In conclusion, the newly developed method for computing RDR *via* the adjoint method can provide the time evolution of the dispersion characteristics of a flow field. The present study helps elucidate the mass or momentum distribution in seas. In future studies, the new method will be applied to real cases in oceans.

## Acknowledgements

Fei Ji thanks the China Scholarship Council (CSC) for supporting his stay in Japan and the Ministry of Education, Culture, Sports, Science and Technology, Japan (MEXT) under a Joint Usage/Research Center, Leading Academia in Marine and Environment Pollution Research (LaMer) Project for supporting his short stay in Japan.

## References

Batchelor, G. K., 1952. Diffusion in a field of homogeneous turbulence II. The relative motion of particles. *Mathematical Proceedings of the Cambridge Philosophical Society*, **48**: 345-362.

Bennett, A. F., 1984. Relative dispersion: Local and nonlocal dynamics. *Journal of the Atmospheric Sciences*, **41** (11): 1881-1886.

Coulliette, C., Lekien, F., Paduan, J. D., Haller, G., and Marsden, J. E., 2007. Optimal pollution mitigation in Monterey Bay based on coastal radar data and nonlinear dynamics. *Environmental Science & Technology*, **41** (18): 6562-6572.

Cucco, A., Quattrocchi, G., Satta, A., Antognarelli, F., De Biasio, F., Cadau, E., *et al.*, 2016. Predictability of wind-induced sea surface transport in coastal areas. *Journal of Geophysical Research: Oceans*, **121** (8): 5847-5871.

Daescu, D. N., and Langland, R. H., 2013. The adjoint sensitivity guidance to diagnosis and tuning of error covariance parameters. *Data Assimilation for Atmospheric, Oceanic and Hydrologic Applications (Vol. II)*. Springer, Berlin, Heidelberg, 205-232.

Davis, R. E., Regier, L. A., Dufour, J., and Webb, D. C., 1992. The autonomous Lagrangian circulation explorer (ALACE). *Journal of Atmospheric and Oceanic Technology*, **9**: 264-285.

Ding, R., and Li, J., 2007. Nonlinear finite-time Lyapunov exponent and predictability. *Physics Letters A*, **364** (5): 396-400.

Dombre, T., Frisch, U., Greene, J. M., Hénon, M., Mehr, A., and Soward, A. M., 1986. Chaotic streamlines in the ABC flows. *Journal of Fluid Mechanics*, **167**: 353-391.

Durgadoo, J. V., Rühs, S., Biastoch, A., and Böning, C. W., 2017. Indian Ocean sources of Agulhas leakage. *Journal of Geophysical Research: Oceans*, **122** (4): 3481-3499.

Errico, R. M., 1997. What is an adjoint model? *Bulletin of the American Meteorological Society*, **78** (11): 2577-2592.

Fiorentino, L. A., Olascoaga, M. J., Reniers, A., Feng, Z., Beron-Vera, F. J., and MacMahan, J. H., 2012. Using Lagrangian coherent structures to understand coastal water quality. *Continental Shelf Research*, **47**: 145-149.

García-Garrido, V. J., Mancho, A. M., Wiggins, S., and Mendoza, C., 2015. A dynamical systems approach to the surface search for debris associated with the disappearance of flight MH370. *Nonlinear Processes Geophysics*, **22**: 701-712.

Gelderloos, R., Haine, T. W., Koszalka, I. M., and Magaldi, M. G., 2017. Seasonal variability in warm-water inflow toward Kangerdlugssuaq Fjord. *Journal of Physical Oceanography*, **47** (7): 1685-1699.

Hackett, B., Comerma, E., Daniel, P., and Ichikawa, H., 2009. Marine oil pollution prediction. *Oceanography*, **22** (3): 168-175.

Haller, G., 2001. Distinguished material surfaces and coherent structures in three-dimensional fluid flows. *Physica D: Nonlinear Phenomena*, **149** (4): 248-277.

Haller, G., 2002. Lagrangian coherent structures from approximate velocity data. *Physics of Fluids*, **14** (6): 1851-1861.

Haller, G., 2015. Lagrangian coherent structures. *Annual Review of Fluid Mechanics*, **47**: 137-162.

Kim, J. J., Stockhausen, W., Kim, S., Cho, Y. K., Seo, G. H., and Lee, J. S., 2015. Understanding interannual variability in the distribution of, and transport processes affecting, the early life stages of *Todarodes pacificus* using behavioral-hydrodynamic modeling approaches. *Progress in Oceanography*, **138**: 571-583.

Kraichnan, R. H., 1966. Dispersion of particle pairs in homogeneous turbulence. *Physics of Fluids*, **9** (10): 1937-1943.

Kuznetsov, L., Toner, M., Kirwan, A. D., Jones, C. K. R. T., Kantha, L. H., and Choi, J., 2002. The loop current and adjacent rings delineated by Lagrangian analysis of the near-surface flow. *Journal of Marine Research*, **60** (3): 405-429.

LaCasce, J. H., and Ohlmann, C., 2003. Relative dispersion at the surface of the Gulf of Mexico. *Journal of Marine Research*, **61** (3): 285-312.

LaCasce, J., 2008. Statistics from Lagrangian observations. *Progress in Oceanography*, **77** (1): 1-29.

Lacorata, G., Palatella, L., and Santoleri, R., 2014. Lagrangian predictability characteristics of an ocean model. *Journal of Geophysical Research: Oceans*, **119** (11): 8029-8038.

Le Dimet, F. X., and Talagrand, O., 1986. Variational algorithms for analysis and assimilation of meteorological observations: Theoretical aspects. *Tellus A: Dynamic Meteorology and Oceanography*, **38** (2): 97-110.

Pierrehumbert, R. T., and Yang, H., 1993. Global chaotic mixing on isentropic surfaces. *Journal of the Atmospheric Sciences*, **50** (15): 2462-2480.

Sanderson, A. R., 2014. An alternative formulation of Lyapunov exponents for computing Lagrangian coherent structures. In: *2014 IEEE Pacific Visualization Symposium*. Yokohama, Japan, 277-280.

Shadden, S. C., Lekien, F., and Marsden, J. E., 2005. Definition and properties of Lagrangian coherent structures from finite-time Lyapunov exponents in two-dimensional aperiodic flows. *Physica D: Nonlinear Phenomena*, **212** (3-4): 271-304.

Shadden, S. C., Lekien, F., Paduan, J. D., Chavez, F. P., and Marsden, J. E., 2009. The correlation between surface drifters and coherent structures based on high-frequency radar data in Monterey Bay. *Deep Sea Research Part II: Topical Studies in Oceanography*, **56** (3-5): 161-172.

**(Edited by Xie Jun)**